Surface x-ray structure analysis of periodic misfit dislocations in Fe/W(110)

R. Popescu, H. L. Meyerheim,* D. Sander, and J. Kirschner
Max-Planck Institut für Mikrostrukturphysik, Weinberg 2, D-06120 Halle, Germany

P. Steadman,† O. Robach, and S. Ferrer
ESRF, BP 220, F-38043 Grenoble, France

(Received 13 January 2003; revised manuscript received 19 June 2003; published 23 October 2003)

We have carried out a surface x-ray diffraction analysis of the geometric structure of a 13-monolayer-thick Fe film on W(110). The Fe adlayer is characterized by a well-ordered two-dimensional array of misfit dislocations that have a periodicity of 35.84 and 50.76 Å along the [001] and [$\bar{1}$10] directions, respectively. In the (110) plane the average Fe structure is isotropically strained by +1.2% with respect to (bulk) bcc Fe, corresponding to lattice constants of 2.901 Å along [001] and 4.103 Å along [$\bar{1}$10]. In the surface normal direction ([110]) we find that the Fe film is also strained by +0.22% ($c=4.062$ Å). This corresponds to a slightly laterally distorted bct phase with $a=b=2.887$ Å, $c=2.901$ Å, and $\gamma=89.4°$. The intensity distribution along 14 satellite rods was analyzed quantitatively using a sine-wave modulation ansatz for the lateral and vertical displacements of the Fe atoms out of their average positions. We find maximum amplitudes in the order of about 0.7 Å for the normal and lateral modulations, respectively. The modulation amplitudes continuously decrease with distance from the Fe/W(110) interface. The adlayer/substrate registry is characterized by a 37/34 coincidence between the Fe- the W atoms, where the vertical Fe corrugation is directly related to the Fe-adsorption site. The implications of the unexpected strain state of the film for its mechanical stress and magnetic anisotropy are discussed.

DOI: 10.1103/PhysRevB.68.155421 PACS number(s): 61.10.−i, 68.35.Ct

I. INTRODUCTION

Owing to its prototype character for the study of structural, mechanic, and magnetic properties, the Fe/W(110) interface is one of the most intensely investigated interfaces in surface science.[1–21] Since the magnetic properties are intimately related to the geometric structure, the investigation of the interface structure as well as the structure within the film remains a primary aim for research. However, quantitative structure analyses are quite rare. Almost 20 years ago Gradmann and Waller[1] investigated the growth of Fe/W(110) using low-energy electron diffraction (LEED) and Auger-electron spectroscopy (AES). Since that time it is generally accepted that the first Fe monolayer (ML) grows pseudomorphically on W(110) (1 ML$=1.41\times10^{15}$ atoms per cm^2). The formation of misfit dislocations begins at higher coverage. The misfit dislocations form a well-ordered two-dimensional lattice, which gives rise to a two-dimensional multiplet of satellite reflections. As an example, Fig. 1(a) shows the LEED image of a 3-ML-thick Fe film. The satellite spots are arranged in diamond-shaped groups around the integer-order reflections of the W(110) substrate. The corresponding scanning tunneling microscopy (STM) image is shown in Fig. 1(b). The different layers (labeled by 2, 3, 4) are represented by the different gray scale. The regularly arranged distortion lines are identified by the vertical corrugation contrast, which is most prominently observed in layer 4.

In later investigations by Bethge *et al.*,[9] Jensen and co-workers,[10] and Sander *et al.*,[16,19] the two-dimensional misfit dislocation network was directly identified by STM and—more indirectly—by a kink in the stress curve measured by the optical bending method. The kink in the stress curve is already observed at about 1.2 ML, however, the long-range ordered dislocation network has been observed only at coverages larger than about 2 ML. In general, misfit dislocations are generated in order to relieve the strain induced in the growing adlayer, which has a different bulk lattice constant than the substrate. The first theory based on a model that treats the adlayer as an elastic continuum, to our knowledge, was developed by Frank and van der Merve.[22,23] For a review of theoretical work on misfit dislocations we refer to Ref. 24. Since the Fe/W(110) interface represents a system with a large misfit of 9.4% ($a_{\mathrm{Fe}}=2.866$ Å, $a_{\mathrm{W}}=3.165$ Å), misfit dislocations are formed at low adlayer thickness ($\approx$1.2 ML). The study of Sander, Enders, and Kirscher[19] has revealed that the formation of misfit dislocations reduces the film stress from more than 40 GPa in the first layer to almost zero in the second and third layers.[20]

However, with regard to the atomic structure of the misfitted adlayer so far only semiquantitative analyses were carried out. In the LEED analysis of Gradmann and Waller[1] kinematic scattering theory was applied to interpret some satellite intensities. Using a first-order sinusoidal modulation wave ansatz for the in-plane displacements, the authors derived a modulation amplitude of about 0.9 Å along the (in-plane) [$\bar{1}$11] direction for a 4-ML-thick film. A detailed layer-dependent analysis of the distortion pattern was not carried out. STM investigations were also not able to develop a full three-dimensional atomic picture of the misfitted Fe adlayer.[9,10,16,19] However, they provided information on the morphology by ascribing the observed STM contrast to the vertical corrugation. The dislocation network could be observed up to 11 ML, which was the maximum thickness investigated in this study. The vertical corrugation amplitude was found to decrease from about 0.7 Å at 4 ML to 0.3 Å at 8 ML.[10]

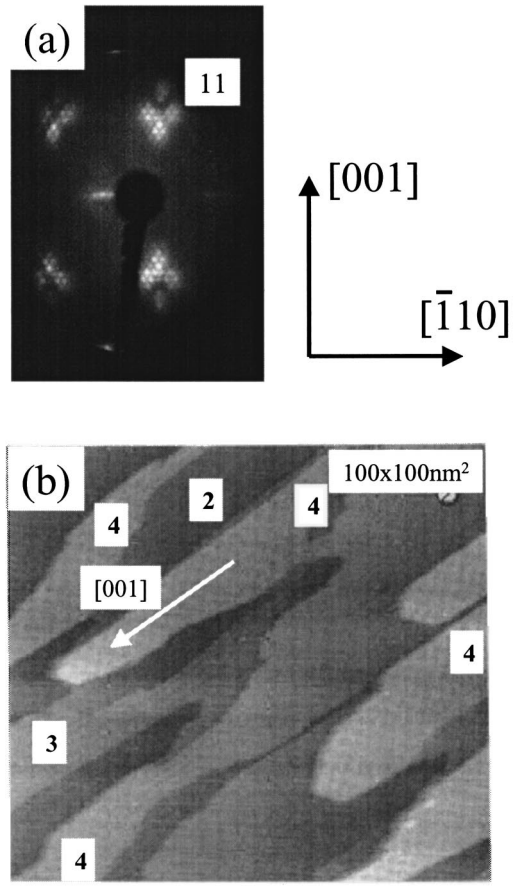

FIG. 1. (a) LEED pattern of a 3-ML-thick Fe film on W(110). The two-dimensional satellite reflection multipletts are arranged in diamond shaped areas around the W(110) main reflections. The electron energy is about 100 eV. (b) Corresponding STM image (100×100 nm^2). The different levels (second, third, and fourth ML as indicated by the labels) are represented by the different contrast. The two-dimensional distortion network is observable at the third and fourth level.

In this paper we present a quantitative surface x-ray diffraction (SXRD) analysis of the misfit dislocation network for a nominally 13-ML-thick Fe film. First, from the positions of the zeroth order satellite reflections, the average in-plane lattice constants of the Fe adlayer are determined to 2.901 ± 0.005 and 4.103 ± 0.005 Å, indicating the presence of an isotropic lateral strain ($\varepsilon_{001}=\varepsilon_{\bar{1}10}=+1.2\%$) with respect to bulk body-centered cubic (bcc) Fe. The strain is also positive for the out-of-plane direction [110], where we find $\varepsilon_{110}=+0.22\%$ (4.062 Å), indicating that the Fe adlayer cannot be simply considered as strained bcc Fe. The unit cell size of the modulated structure along both in-plane directions is larger by a factor 11.33 ± 0.01 than the respective lattice constants of the W(110) surface, 50.76 Å (versus 4.476 Å for W) along [$\bar{1}$10] and 35.84 Å (versus 3.165 Å for W) along [001]. The noninteger ratio 11.33 ± 0.01 indicates an incommensurate Fe superstructure. While the lattice parameters of the modulated Fe structure and the W substrate are not given by a ratio of integers, the $\sqrt{2}$:1 ratio between the in-plane lattice constants is preserved in the film as expected for a (110) bcc film.

A three-dimensional atomic structure model based on the quantitative interpretation of the intensity distribution along 14 symmetrically independent satellite rods is developed. We find that the normal corrugation decreases from about 1.2 Å for the Fe layers next to the W(110) surface to about 0.3 Å for the outermost Fe layer. The in-plane modulations decrease from 0.7 Å in the second layer to 0.3 Å.

This paper is organized as follows: Section II briefly outlines the most important experimental details and Sec. III discusses the structure analysis as far as the lattice geometry is concerned. Sections IV and V deal with the quantitative intensity analysis and the discussion of a structure model. The impact of the peculiar film strain on film stress and magnetic anisotropy are discussed in Sec. VI.

II. EXPERIMENTAL ASPECTS

The experiments were carried out at beam line ID3 of the European Synchrotron Facility (ESRF) in Grenoble using a six-circle ultrahigh-vacuum diffractometer operated in the *z*-axis mode[25] at a wavelength of 0.73 Å. The W(110) surface was cleaned by heating the sample several times at 1500 °C in 10^{-6} mbar oxygen partial pressure for 30 s. After a final flash at 2000 °C for 10 s the C contamination of the surface is lower than 1% of a ML as determined by AES. The thickness calibration was carried out using a quartz oscillator and by observing the SXRD intensity oscillations of the (001) crystal truncation rod (CTR) reflection.[26,27] Since the latter are observed up to a coverage of about 2 ML due to the onset of island growth, the thickness calibration for thicker layers (>5 ML) is less accurate. Here we rely on a constant deposition rate, as checked during deposition by monitoring the Fe ion flux, and the constancy of the calibration parameters. In total 13 Fe layers were deposited *in situ* by electron-beam evaporation from a high-purity rod. In this context it must be emphasized that this coverage is derived from the present SXRD analysis, which only yields the number of layers, which contribute to the modulated structure. Our previous SXRD analysis in the low-coverage regime[26] as well as from the Mössbauer analysis[4] of thicker films (up to about 11.5 ML) have indicated the presence of about two pseudomorphic layers next to the W(110) surface. Since they do not contribute to the satellite intensities they are not considered in the present analysis.

The sample was slightly annealed after deposition in order to optimize the structure quality as measured by the peak intensity and the full width at half maximum (FWHM) of the first-order Fe reflection, which is related to the average Fe structure (see below). It increased by nearly 100% upon annealing. However, the transverse FWHM decreased only from 0.8° to 0.6° (corresponding to $\Delta q_{\parallel}=4.4\times10^{-3}$ Å^{-1}, omitting the factor 2π), which translates into a domain size of about 23 nm. We conclude that the annealing process does not primarily increase the average island size, but rather leads to an ordering of a substantial amount of Fe, which was not in registry with the deposited Fe film before annealing.

Figure 2(a) gives an overview of the (*hk*) plane of reciprocal space of the Fe-covered W(110) surface. The inset in

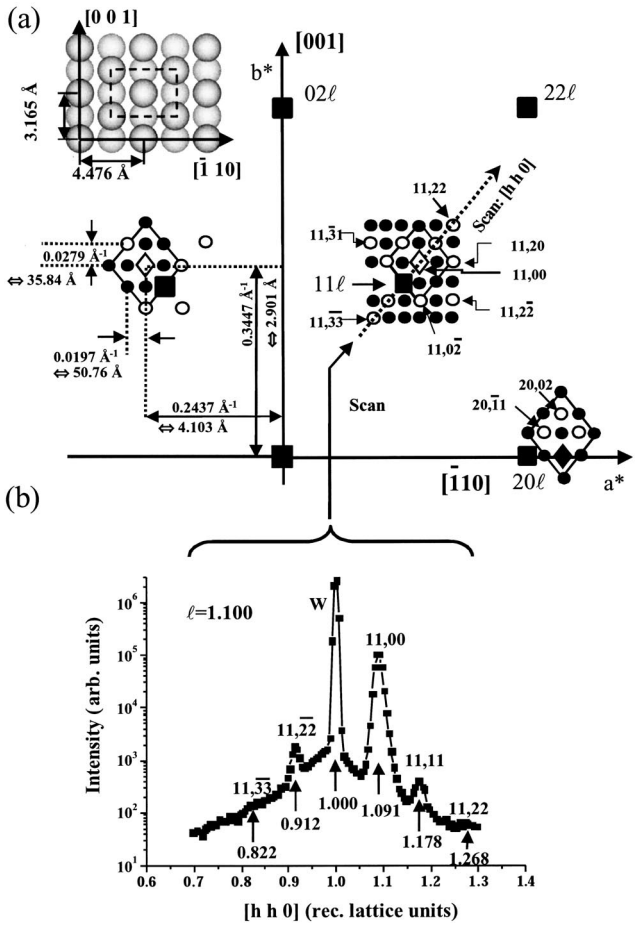

FIG. 2. (a) Schematic view of the W(110) surface (upper left) and the reciprocal lattice of the Fe/W(001) film in the a^*-b^* plane. The large squares represent the W CTR's. The Fe satellite reflections are represented by circles and diamonds, the latter represent the zero-order satellites related to the average film structure. Open symbols indicate reflections used for the analysis. In the left part of the figure some distances are given. (b) Intensity profile along the $[hh0]$ direction in reciprocal space measured at $q_z = 1.10$ r.l.u. [see arrow in (a)]. The Fe satellite reflections are indexed above the peaks; the h coordinate within the W coordinate system is given below the reflections.

the upper left shows the atomic arrangement of the W(110) surface. The dashed rectangle indicates the (centered) surface unit cell. The lattice directions are related to the bulk setting of (bcc) W. The reciprocal-lattice vectors are chosen so that the a^* and b^* axes are parallel to $[\bar{1}10]$ and [001], respectively. In the sketch of the reciprocal space, the large squares represent the integer-order CTR's of the W(110) substrate, which are indexed according to the face centered (fc) setting of the W unit cell. The circles are the non-zero-order satellite reflections related to the modulation of the Fe layer. The diamonds represent the zero-order satellites related to the average Fe-film structure. Owing to the lack of translation periodicity along the surface normal, all reflections are extended to rods along the normal direction, [110], $q_z = lc^*$, with $c^* = 1/(4.476\ \text{Å}) = 0.223\ \text{Å}^{-1}$. Consequently, the reflection index (l) is a continuous parameter.[27] Indexing of the satellite reflections can be done in two different ways. First, all reflections can be related to the W-substrate lattice. This is convenient in order to directly analyze the lattice metric of the Fe film with respect to the W substrate (see Sec. III). On the other hand, for the analysis of the satellite reflection intensities (Sec. IV) the spots are labeled by using the five-character symbol (hkl,mn). The index hkl labels the main reflection next to the satellite indexed by mn. The condition $m = n = 0$ refers to the zero-order satellite. In Fig. 2(a) some satellites are indexed in this way, where the third coordinate l has been omitted for clarity.

Integrated x-ray reflection intensities were collected by transverse scans up to a maximum normal momentum transfer of $l = q_z/c^* = 2.25$ reciprocal lattice units (r.l.u.). The transverse width of the reflections is given by the sample domain size (≈23 nm, see above), while the out-of-plane resolution is determined by the setting of the detector slits. In the present experiments it is approximately $4.7 \times 10^{-3}\ \text{Å}^{-1}$ corresponding to 0.02 r.l.u. along c^*. Only the intensities of those reflections labeled by an open symbol in Fig. 2(a) were taken into account for the structure analysis. Systematic scans in the vicinity of the main reflections showed that no intensity was observed for those reflections, fulfilling the condition $m + n = 2\mu + 1$ (μ integer), indicating a centered supercell lattice symmetry. Other (symmetry-allowed) reflections with $m + n = 2\mu$, but more distant from the main reflections, were found to be too weak to be measured in general. In total 222 reflections were measured and subsequently reduced to 188 by symmetry equivalence. The structure factor amplitudes $|F(hkl,mn)|$ were obtained after correcting the intensities for effective sample area, Lorentz factor, and polarization factor.[28] The standard deviations (σ) of the $|F|$ values were derived from the reproducibility of symmetry-equivalent reflections and the counting statistics.[29,30] In general, they are in the 10–20 % range, which—considering the large fraction of weak reflections—is a reasonable value.

III. GEOMETRIC ANALYSIS

The geometric parameters of the modulated structure were derived as the first step of the analysis. The positions of the satellite reflections could be determined with very high accuracy from the positions of the (1×1) W CTR's, which serve as an internal reference. Figure 2(b) shows on a logarithmic scale the intensity measured along the $[hh0]$ direction in reciprocal space. The normal momentum transfer was kept constant at $q_z = 1.10$ r.l.u. In Fig. 2(a) the scan direction is shown by the dotted arrow starting from the $(11,\bar{3}\bar{3})$ satellite and ending at the (11,22) satellite. The scan also crosses the W-crystal truncation rod (11) and the zero-order satellite, (11,00), of the modulated structure. The coordinates $(h, k = h)$ of the reflections related to the W-coordinate frame are listed below the peaks.

From the position $(h = k = 1.091 \pm 0.002)$ of the zero-order satellite, the in-plane lattice constants of the (average) Fe adlayer are directly derived to 4.103 ± 0.005 Å along $[\bar{1}10]$ and 2.901 ± 0.005 Å along [001], respectively. Compared with the respective values of bulk bcc Fe (4.053 and 2.866 Å) this indicates an in-plane strain of +1.22% along

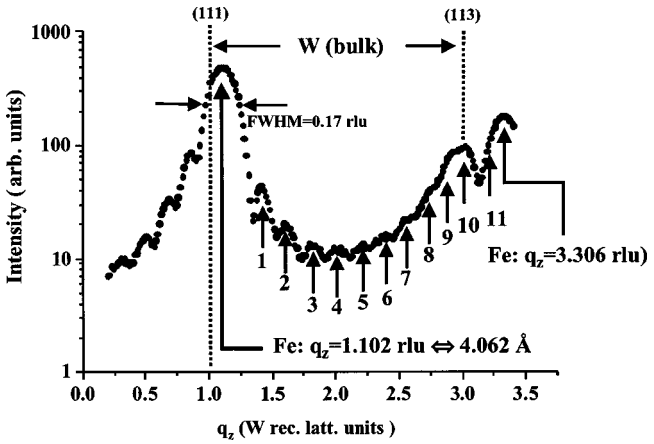

FIG. 3. Scan along q_z of the zero-order satellite reflection of the Fe layer located at (1.091, 1.091) within the W coordinate frame (see also Fig. 2). The dashed lines at $l=1$ and 3 indicate the bulk W reflection positions along the neighboring (11l) W CTR. Between the Fe main reflections at $l=1.102$ and 3.306 r.l.u., there are 11 side maxima, indicating an Fe thickness of 13 layers.

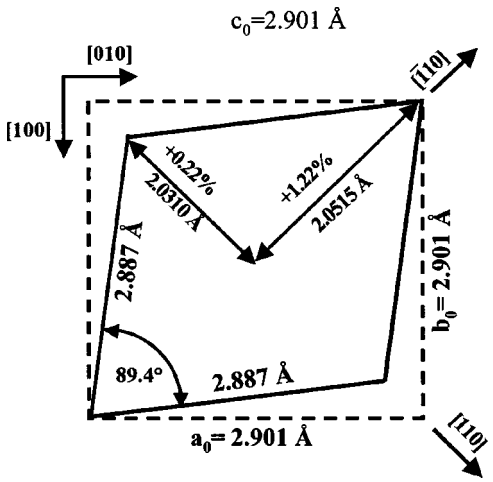

FIG. 4. Sketch visualizing the distortion (grossly exaggerated) of the average Fe-film lattice metric projected along [001]. The dashed square represents the cubic case with $a=2.091$ Å, the lattice constant of the film along [001]. The solid rhombus is the unit-cell shape of the average structure in the [100]-[010] plane. Lattice parameters and expansions (in percent relative to bcc Fe) are indicated.

both in-plane directions. The magnitude of the strain does not depend on whether the film was annealed after deposition or not. During the course of the experiments we determined the same strain values also for a nominally 5-ML-thick layer.

The vertical lattice metric is derived from the intensity distribution along the surface normal. Figure 3 shows on a logarithmic scale the intensity distribution of the (11,00) zero-order satellite along q_z. The dashed lines at $l=1$ and $l=3$ r.l.u. mark the positions of the W-bulk reflections along the neighboring (11l) CTR. These satisfy the reflection condition (h,k,l) all even or odd according to the face-centered (fc) setting of the W unit cell. Due to the strong W-bulk reflection at (113) there is some distortion of the measured satellite intensity around $l=3$ since the W(11l) CTR is close to the satellite rod (1.091,1.091,l) within the W coordinate frame. However, for the geometric analysis of the structure, this is not relevant. Important results are directly derived from an inspection of the intensity distribution of Fig. 3.

The Fe-surface structure adopts the substrate lattice type, i.e., the Fe film grows with its (110) face on the W(110) surface. The ''Bragg'' peaks along the (11l,00) satellite rod located at $l=1.102$ and 3.306 r.l.u. correspond to the reflection condition for a fc lattice in analogy to the W(11l) CTR and translate to a lattice constant of 4.062 Å (=4.476 Å/1.102). Again, the comparison with bulk Fe (4.053 Å) indicates an *expansion* of the average Fe structure by 0.22% along the film normal [110]. Using the bulk Fe elastic constants[31] one would expect a -0.82% *contraction* as a consequence of the 1.22% in-plane expansion. Thus, the Fe film under investigation is not simply strained bcc Fe but resembles an enlarged atomic volume. An in-plane strain of $+1.22\%$ and a contraction of -0.82 would result in a relative volume change of $\Delta V/V=\varepsilon_{11}+\varepsilon_{22}+\varepsilon_{33}=1.22+1.22-0.82=1.62\%$, while our analysis yields $\Delta V/V=\varepsilon_{11}+\varepsilon_{22}+\varepsilon_{33}=1.22+1.22+0.22=2.66\%$.

In order to clarify the metric in more detail, Fig. 4 schematically shows the lattice parameters of the average film structure in the projection along [001]. The dashed square represents the theoretical case of a cubic unit cell with $a=b=c=2.901$ Å. Note that $c=2.901$ Å is the lattice parameter determined along the [001] direction. The square serves as a guide for the eye to better clarify the lattice distortion. The solid rhombus represents the unit cell according to our SXRD measurements. The lengths 2.0310 and 2.0515 Å are given by the measured lattice constants along [110] and [$\bar{1}$10], respectively. Note that the two corners of the rhombus pointing along $\langle\bar{1}10\rangle$ coincide with the dashed square, since along both the [$\bar{1}$10] and the [001] directions the lattice strain is $+1.22\%$. Using the measured lattice parameters, the edges of the rhombus are 2.887 ± 0.004 Å (bulk bcc Fe, 2.866 Å), while the angle γ is derived as $89.4\pm0.1°$. Note that the distortion characterized by the angle $\gamma\neq90°$ is a very tiny effect and that the drawing grossly exaggerates the real situation. In summary, the unit cell of the average Fe-film structure can be viewed as a slightly laterally distorted volume expanded bct phase, which has no direct relation to other (metastable) lattice such as fcc or hexagonal close packed (hcp).[32]

Information on the film thickness (d) is derived from the FWHM of the first Bragg peak, which is 0.17 r.l.u. $=0.038\,\text{Å}^{-1}$ (see Fig. 3). Using the relation $d=1/(0.038\,\text{Å}^{-1})$ we find $d=26.3$ Å. This corresponds exactly to 13 layers of 2.02 Å thickness, which is close to the average layer thickness of 2.031 Å (=4.062/2 Å) as derived above. A further confirmation of the layer thickness comes from the observation of $M=11$ well-defined side maxima (corresponding to $M+2=13$ layers[33]) between the two main maxima. In Fig. 3 the side maxima are indicated by the arrows and numbered from $M=1$ to $M=11$.

So far we have discussed the average structure of the Fe film. The metric of the modulated (super-) structure is de-

rived from the spacing between the satellite spots [see left part of Fig. 2(a) where the distances are given]. Along $[\bar{1}10]$ and [001] these are determined to be $\Delta q_{[\bar{1}10]}=0.0197 \pm 0.0003$ Å^{-1} and $\Delta q_{[001]}=0.0279\pm 0.0002$ Å^{-1}, respectively. Accordingly, the modulation periodicity (MP) is $a_{\mathrm{MP}} =50.76\pm 0.50$ Å along $[\bar{1}10]$ and $b_{\mathrm{MP}}=35.84\pm 0.50$ Å along [001]. The relationship between the W(110) lattice and the modulated film is expressed by the ratio $p=a_{\mathrm{MP}}/a_{\mathrm{W}} =b_{\mathrm{MP}}/b_{\mathrm{W}}=11.33\pm 0.01$. This value indicates that the modulated supercell is incommensurate with the W(110) unit cell. However, the $\sqrt{2}$:1 ratio between the W lattice parameters along $[\bar{1}10]$ and [001] (4.476 and 3.165 Å) is preserved in the adlayer and reflects the intimate relation between the Fe film and the substrate.

We conclude that the Fe film is characterized by a well-ordered and homogeneous structure with no significant (depth-dependent) disorder. The average lattice constant of the film is larger than that in bulk Fe, and it is given by an isotropic in-plane strain of $+1.22\%$ and an out-of-plane strain of $+0.22\%$.

IV. INTENSITY ANALYSIS

In order to refine the analysis and to develop a three-dimensional structure model for the modulated Fe-film structure the intensity distribution along the satellite rods was analyzed quantitatively. The structure factor amplitudes $|F|$, of seven out of 14 satellite rods together with their standard deviations σ are shown in Figs. 5(a)–5(g) as solid symbols. The rods are labeled according to the convention discussed in Sec. II. Note the huge intensity (I) variation within the data set, which is of the order of 10^3 between the strongest and the weakest reflections ($I\propto|F|^2$). The solid lines correspond to the best fit to the data as will be discussed in the following.

The analysis is based on describing the structure in terms of modulation waves. The ν-th atom in the modulated structure, which is located at $\mathbf{r}_\nu$, is shifted by $\mathbf{u}_\nu$ out of its average position $\mathbf{r}_\nu^0$ according to the relation $\mathbf{r}_\nu=\mathbf{r}_\nu^0+\mathbf{u}_\nu$. In this approach, the average structure is modeled using the bulk stacking of the Fe layers. Within the unit cell (see the model in Fig. 2) the symmetry independent W atoms are at (0,0,0) and $(\frac{1}{2},0,\frac{1}{2})$. Note that there are two atoms per unit cell in each layer ($\nu=2$); only one of them is independent due to the centering of the unit cell (plane group $cmm2$). The shift of the Fe atoms out of their average positions can be described by using a harmonic modulation function, which in the most general case is given by[34]

$$u_\nu=\sum_i U_\nu^s(i)\sin[2\pi Q_i(n+g_\nu)] + \sum_i U_\nu^c(i)\cos[2\pi Q_i(n+g_\nu)]. \quad (1)$$

In Eq. (1) the U_ν's and $\mathbf{Q}_i$'s represent the amplitudes and the modulation vectors of the sine (s) and cosine (c) displacement waves, respectively. The parameters g_ν are the phases

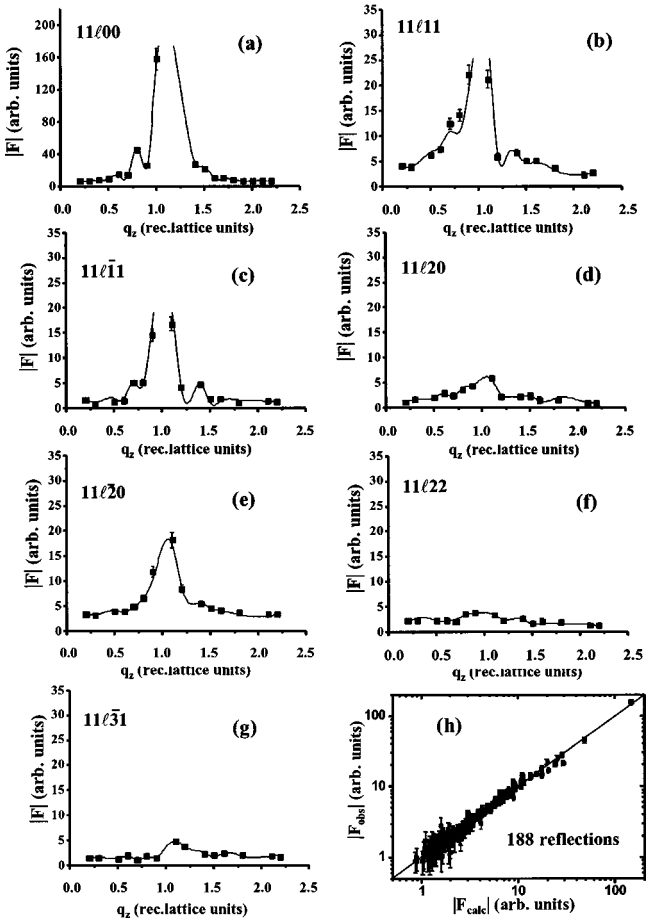

FIG. 5. (a)–(g) Measured (symbols) and calculated (lines) structure factor amplitudes for seven of 14 satellite reflections along q_z. The rods are indicated according to Fig. 2. (h) Plot of $|F_{\mathrm{obs}}|$ vs $|F_{\mathrm{calc}}|$ for all 188 reflections. The data are closely aligned along the diagonal corresponding to the condition $|F_{\mathrm{obs}}|=|F_{\mathrm{calc}}|$.

of the atoms (ν) within the unit cell and n (integer) represents a lattice translation. For the analysis we have chosen two (orthogonal) in-plane modulation basis vectors: $\mathbf{q}_1 =(0.0809,0.0)$ and $\mathbf{q}_2=(0.0,0.0809)$. The choice is based on the minimum spacing between the satellite reflections, which is 0.0882 r.l.u. along both in-plane directions within the W coordinate frame (see Fig. 2), which is equivalent to 0.0809 r.l.u. within the Fe coordinate frame. Higher-order modulation vectors can be taken into account by linear combinations of $\mathbf{q}_i$ according to $\mathbf{Q}_i=\Sigma_j\alpha_{ij}\mathbf{q}_j$, with α_{ij} integer. The structure refinement was carried out by using a limited set of modulation waves using the components $\alpha_{ij}=(2,0)$, (0,2), (4,0), (0,4), (1,1), (2,2), (3,1), and (1,3) and their symmetrically equivalent components corresponding to the $pmm2$ point-group symmetry. This set corresponds to 20 modulation waves (Q_i) in total. Symmetry restrictions according to the five-dimensional space group 851 labeled by $cmm2(q00,0p0)mm0$ in Ref. 35 are implemented in the refinement program JANA 2000,[36] which was used throughout the analysis. The $cmm2$ symmetry of the supercell is confirmed by the extinction of those satellites with the condition $m+n=2\mu+1$ as discussed in Sec. II.

Despite the convenient approach to describe the structure in terms of modulation waves, the number of variables is too large in relation to the number of observed reflections. In detail, for each of the 13 layers there is one (positional) z parameter and 12 lateral and 6 vertical modulation amplitudes. Together with one overall scale factor this adds up to in total $19\times13+1=248$ free parameters to refine, which even exceeds the number of reflections (188). In order to simplify the analysis, a modulation amplitude profile within the film is constructed assuming a simple functional relationship of the (total) modulation amplitudes $u(N)$ [see Eq. (1); dropping the index ν] of the layers. For example both, experiment[9] and theory[23] proposed that the modulation amplitude in the film decreases with increasing distance from the interface. Treating the film as an elastic continuum, van der Merve found an exponential decrease of the distortions with increasing film thickness. This can be described by the z-dependent modulation, $u(z)=u_0\exp(-2\pi z/p)$, where p and z represent the modulation periodicity and the distance of the layer from the interface, respectively. The parameter u_0 corresponds to the maximum modulation, which affects the first layer next to the substrate (or the pseudomorphic layers in the present case). The theory—although originally developed for the case of a one-dimensionally misfitted adlayer—is also applicable for distortions in two-dimensional epitaxial layers, provided that the films grow in a layer-by-layer mode and the two-dimensional symmetries of substrate and film are identical. To first order both prerequisites are fulfilled in the present case; however, it might be questionable whether the film can be considered as an elastic continuum at this coverage.

Starting with this idea we fitted the intensity data by using u_0 and p as fit parameters, while the distance z of the layer from the substrate (including the pseudomorphic layers) is given by $z=N\bar{d}$, where $\bar{d}=2.031$ Å is the average layer spacing within the Fe film and N the number of the Fe layers. However, this approach did not immediately lead to very satisfying results. Therefore in a second step an improvement of the fits was tried by allowing for some deviations of the distortion amplitudes from the exponential decay. Furthermore, the minimum interatomic Fe distances were constrained not to vary more than about 10% from the bulk value (2.48 Å). On the basis of this approach, the data could be fitted with high accuracy [see solid lines in Figs. 5(a)–5(g)] as expressed by the unweighted residuum (R_u) of 0.09.[36] This also evident from Fig. 5(h) where all 188 observed structure factor amplitudes ($|F_{\mathrm{obs}}|$) are plotted versus the calculated ($|F_{\mathrm{calc}}|$) ones. The data are closely aligned along the diagonal line representing the condition $|F_{\mathrm{obs}}|=|F_{\mathrm{calc}}|$. This is noteworthy, since there is a large intensity dynamics within the data set and only one overall scale factor was used; this corroborates the physical relevance of our model. The final structure model is outlined in Figs. 6–8.

V. MODEL OF THE FILM STRUCTURE

Figure 6(a) compares a calculated vertical corrugation plot based on the refined structure model with a previously measured STM image [Fig. 6(b)].[37] Since the experimental

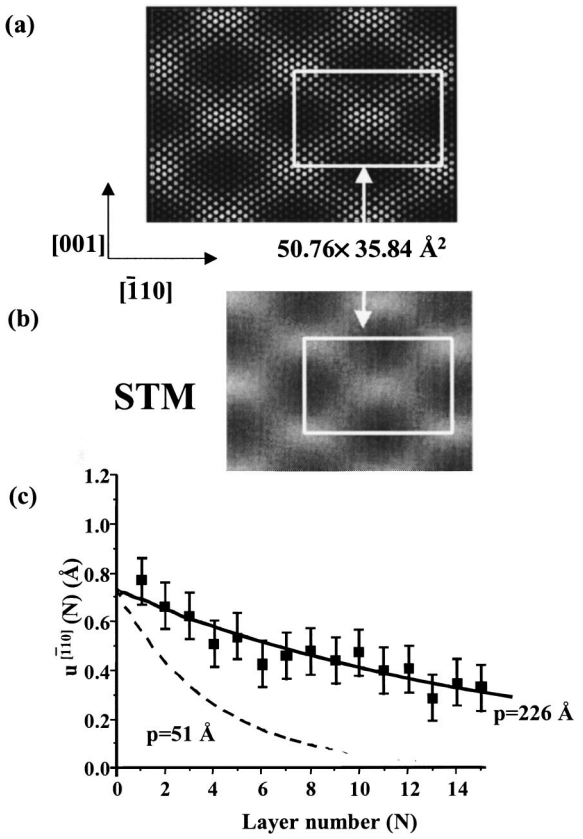

FIG. 6. (Color online) (a) Simulated and (b) measured STM images (Ref. 37) for 4-ML Fe/W(110). The simulated image is derived from the results of structure refinement for the fourth layer. The solid rectangle indicates one unit cell of the modulated structure. (c) Layer-resolved longitudinal modulation amplitude along [$\bar{1}$10]. The solid and dashed lines represent theoretical modulation amplitudes on the basis of an exponential decay with different damping factors p (see text).

STM image is obtained from a 4-ML sample we show the fourth layer of the film. We are aware that this comparison generally needs a caveat, since in our investigation the layers are buried by a number of overlayers, while the STM analysis always probes the top layer. Consequently, the modulations need not be equivalent. Nevertheless, to first order we assume that the effect of the overlayers on the modulations of the deeper layers is—if present at all—small. Therefore the comparison between SXRD and STM appears reasonable.

The brightness of the spheres (Fe atoms) represents vertical corrugation in analogy to a STM image. The solid rectangles indicate the unit cell of the modulated structure (50.76×35.84 Å^2). First, there is a very close resemblance between the images, showing that the STM contrast is related to the corrugation of the Fe atoms. This directly indicates that there are no significant modifications induced in the layer structure upon deposition of subsequent adlayers as mentioned above. Closer inspection of the image also reveals lateral two-dimensional modulation, whose amplitudes are on the order of several tenths of an angstrom. In general,

along both in-plane directions, $[\bar{1}10]$ and [001], there are three waves: one longitudinal and two transversal waves. These are described by the Q_i-dependent amplitudes $U(i)$ of the different waves (i) coherently adding up to the total modulation u [see Eq. (1) and the subsequent discussion]. Figure 6(c) shows $u^{[110]}(N)$, the longitudinal modulation amplitude of the different layers (N) along $[\bar{1}10]$. The parameter N runs from 1 to 15. Note that two additional top layers ($N=14,15$) with fractional occupancies of about 0.4 and 0.2, respectively, were introduced, which led to an improved fit quality. These extra layers represent some islands on top of the Fe film. This is an experimentally supported assumption, because the Fe film growth is not perfectly layer-by-layer and some islands remain on top of the last filled layer even after annealing.

The data analysis reveals that the modulation amplitude $u^{[\bar{1}10]}(N)$ is slowly decreasing from the maximum value in the range of 0.7 Å for the layers next to the W(110) surface to about 0.4 Å for the top layers. The error bars for $u^{[\bar{1}10]}\times(N)$ are estimated to be ± 0.15 Å. The solid and dashed lines in Fig. 6(c) are calculated profiles according to the exponential decay $u(z)\propto\exp(-2\pi z/p)$, using $p=226$ and $p=51$ Å, respectively. The latter corresponds to the modulation periodicity along $[\bar{1}10]$. The fitted data closely follow the $p=226$ Å curve, indicating a much less pronounced damping of the distortion as compared to the van der Merwe theory. This certainly can be attributed to the question of whether the assumptions made by theory are valid in the present case. For example, treating the film as an elastic continuum requires the condition $d \gg a_{\mathrm{Fe}}$, where d is the total thickness of the adlayer and a_{Fe} the Fe lattice constant. This condition is hardly fulfilled in the present case. We can also compare our results with the experimental data of Ref. 1. In this study, $u=0.9$ Å was found for a 4-ML sample along the $[\bar{1}11]$ direction based on the observation that the intensity of the zero-order Bessel function (proportional to the reflection intensity of the average structure) is at a minimum at this coverage. This compares to 0.65 Å in our study when calculating the average value over the first four layers of the modulation amplitude along $[\bar{1}11]$ from our data. This is a fair agreement keeping in mind that the LEED analysis cannot distinguish between the different vector components of the modulation and averages over the layers.

Next, we discuss the layer-resolved vertical corrugation $[\rho(N)]$ within the film structure. The corrugation $\rho^{[110]}(N)$ is the peak-to-peak height difference of the atoms in a given layer (N) and is directly related to the vertical (transversal) modulation amplitude, $u^{[110]}(N)$. Roughly, ρ is about a factor of 2 larger than $u^{[110]}(N)$. Choosing the corrugation instead of the modulation amplitude allows a direct comparison of the results with STM data. Figure 7(a) shows the model of the film structure in the corresponding section, while the filled triangles in Fig. 7(b) represent the layer-resolved corrugations. It should be noted that Fig. 7(a) only shows the modulated part of the structure (i.e., excluding the substrate and the pseudomorphic layers). Thus, in the analysis it is assumed that the substrate and the pseudomorphic

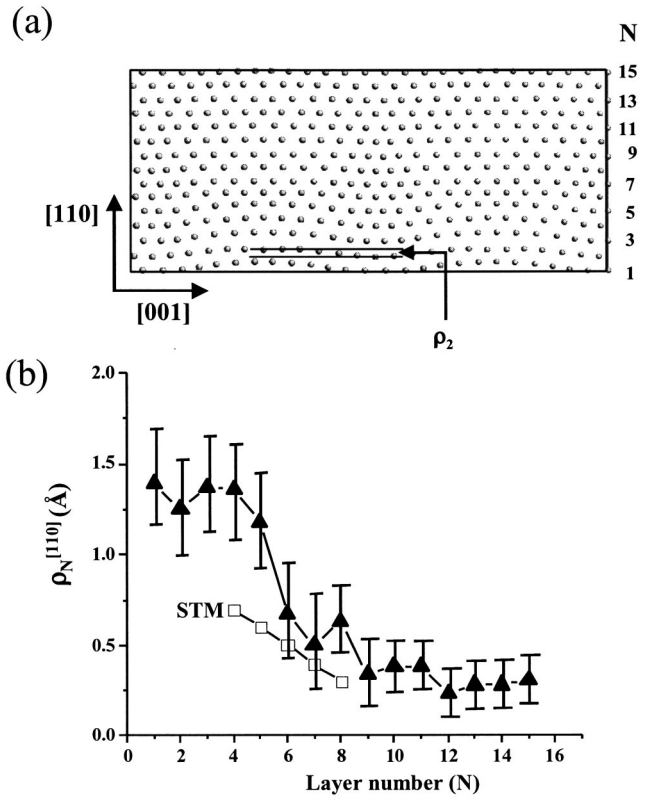

FIG. 7. (a) Structure of the Fe film in the [001]-[110] plane. The layers are numbered on the right. (b) Corrugation amplitude ($\rho^{[110]}$) for the Fe layers as derived from the fits (solid symbols). The open symbols are taken from the STM analysis of Ref. 10 for comparison.

layer(s) are not modulated by the adlayer. With consideration of the strong bonding between Fe and W (i.e., the first pseudomorphic layer and the surface) and the generally observed rapid damping of structural relaxations in metals, this assumption appears justified.

The corrugation $\rho^{[110]}(N)$ is in the range of about 1.3 ± 0.3 Å for the first five layers and drops rapidly to the 0.6–0.4-Å range for the following layers. Due to the comparatively large error bars, we cannot clearly decide whether the apparent constancy of $\rho^{[110]}(N)$ for $N=1$ to 5 is an artifact or whether it is a characteristic of the structure. Nevertheless, as in the case of the lateral modulation, we observe a general decrease of $\rho^{[110]}(N)$ with the distance from the Fe-W interface in agreement with expectations. Other models, such as assuming constant $\rho^{[110]}(N)$ as well as step profiles of significantly different amplitudes, always lead to significantly worse fit qualities (e.g., R_u in the order of 0.2–0.3). This directly shows the reliability of the $\rho^{[110]}(N)$ profile.

The decay of $\rho^{[110]}(N)$ vs N is also observable in the structure model in Fig. 7(a). In general, the layer $N+1$ is located above the layer N so as to achieve a maximum of ''pseudomorphism,'' i.e. in order to preserve as good as possible the local hollow-stacking of the atoms within the film and to avoid additional dislocation lines. We may speculate that—at least to the coverage investigated-the preservation of the local hollow-stacking within the film and the related slow

damping of the distortions is preferred over a rapid relaxation of the modulated structure to an undistorted one. This is most likely due to the high energy cost of considerable local distortions which are inevitably connected with a more rapid damping of the modulation.

The corrugation can be compared quantitatively with STM data measured on a wedge-shaped sample in the 4–8-ML range.[9,10] The analysis of the height distribution (based on the full width at half maximum) within each ML revealed a vertical corrugation of about 0.7 Å for the fourth layer, which slowly decreased to about 0.3 Å for the eighth layer. In Fig. 7(b) the STM results are displayed by the open symbols for comparison. Within the error bars there is fair correspondence for the layers $N=6-8$; however, for the layers 4 and 5 the SXRD analysis derives larger corrugations. The reason for the deviations between STM and SXRD is not clear at present. On one hand, one could argue that the STM contrast does not in general correspond to the geometric corrugation; on the other hand, the SXRD-derived corrugation in the 1-Å range is at the upper limit, which is justified from simple geometric considerations.

A hard-sphere model gives further insight. The maximum corrugation for Fe deposited on the W(110) surface is obtained if the Fe atoms are placed in both hollow and on-top sites. Assuming for simplicity atomic radii for Fe and W as 1.26 and 1.40 Å, respectively,[38] the height difference between these sites is $2.66-2.14=0.52$ Å, which is significantly lower than our observation. Using experimentally derived adsorption heights for Fe in the hollow site (keeping the top site adsorption height at the theoretical value),[5,6,26] the corrugation increases to 0.72 Å, which still is somewhat lower than the corrugation derived for the modulated Fe film.[39] Thus, it seems that the SXRD analysis slightly overestimates the corrugation (at least within the deeper layers). One can speculate that this is related to the simplifications necessary to carry out the intensity refinement, such as the limited number of modulation waves.

So far, we have discussed the structure of the Fe film only, since on the basis of the measured satellite intensities it is not possible to derive the registry between the film and the underlying W substrate including pseudomorphic layers. This is due to the fact that the W substrate as well as pseudomorphic layers only contribute to the W-(1×1) CTR's but not to the satellite reflections. Nevertheless, by using the symmetry, the lattice parameters, and the structure of the modulated film, it is possible to develop a reasonable model for the adlayer registry, which is shown in Fig. 8. The small black circles represent the W atoms of the unrelaxed (110) surface, while the larger circles are the Fe atoms of the first modulated adlayer. In the same way as in Fig. 6(a) the brightness of the Fe atoms represents the corrugation. Note that for presentation purposes, the stacking is reversed, i.e., the Fe atoms are below the W atoms. From Fig. 8 it is directly clear that the vertical Fe corrugation can be related to the local Fe-adsorption position. Fe atoms in bridge and hollow sites are located at lower *z* positions and are represented by darker circles than those next to on-top sites. The Fe/W registry is chosen so as to place one Fe atom exactly on top of one W atom (indicated by the arrow). Following this row of atoms

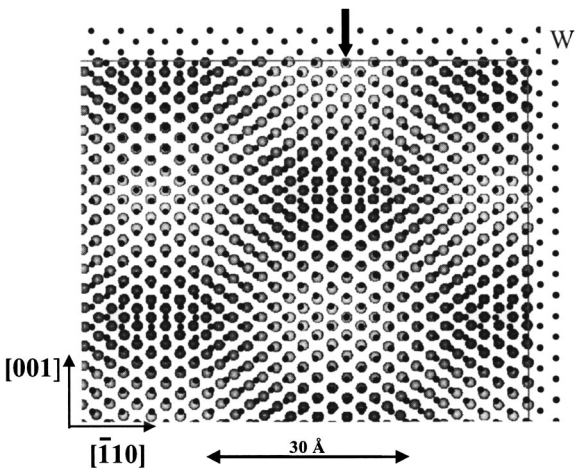

FIG. 8. (Color online) Model of the film registry relative to the W(110) surface. Black and bright circles correspond to W and Fe atoms, respectively. The brightness of the Fe atoms corresponds to their vertical corrugation emphasizing the direct relation of the vertical position with the respective adsorption sites. The W atoms are drawn on their regular bulklike positions with no relaxation.

along the negative [001] direction, the Fe atoms continuously shift out of the top position to the hollow position and back to a near-top position after 12 interatomic distances of the W lattice. The next (close to) on-top position is occupied by the 13th Fe atom in this row. This roughly corresponds to a 13/12 (=1.0833) coincidence between Fe and W. The more accurate value from the geometric analysis of the satellite reflection positions yields $r=1.0882$, corresponding *approximately* to a 37/34 coincidence, which, however, cannot be extracted from the plot due to the limited accuracy.

VI. IMPLICATIONS FOR FILM STRESS AND MAGNETIC ANISOTROPY

In the following we discuss first the implication of the unexpected strain anisotropy for the mechanical stress of the Fe film, which we have measured previously.[20] Then, we conclude with a discussion of the strain-induced contribution to the magnetic anisotropy of the Fe film, which has been discussed by Elmers and Gradmann[6] under the assumption of a strain state, which differs from our strain analysis.

Our structural analysis proposes an isotropic tensile in-plane film strain, $\varepsilon_1'=\varepsilon_2'=0.012$, which is accompanied by a tensile out-of-plane film strain, $\varepsilon_3'=0.0022$, where the primes indicate film properties. This finding is in contrast to the expectations of continuum elasticity.[18] Usually, the strain perpendicular to the film ε_3' is regarded as a free parameter, which is set to minimize the elastic energy density f_{el} with respect to ε_3'. This corresponds to the idea of a zero stress in the direction perpendicular to the film plane, i.e., $\partial f_{\mathrm{el}}/\partial\varepsilon_3'=\tau_3'=0$, and this assumption requires ε_3'(expected) $=-0.0082$ for the given in-plane strain of $\varepsilon_1'=\varepsilon_2'=0.012$. Thus, continuum elasticity predicts that the positive in-plane strain should be accompanied by a negative strain along the film normal. However, our strain analysis results in a positive strain also along the film normal. An immediate consequence

is a larger atomic volume (+2.6% as compared to bulk Fe) for Fe in the experimentally determined strain-state as compared to the calculated strain state based on continuum elasticity (+1.6% as compared to bulk Fe). The occurrence of tensile strain along three orthogonal directions leaves Fe in a less tetragonally distorted environment, as compared to the compressive strain along the film normal, which is calculated by continuum elasticity from the in-plane tensile strain. This is especially important for the calculation of those film properties, which depend on the deviation of the film structure from the cubic symmetry, as does the strain-induced magnetic anisotropy, which will be discussed below. But also the calculation of film stress depends on the strain state, and this aspect is discussed next.

The film stress components τ_i' are calculated from the respective derivatives of the elastic energy density $\partial f_{\mathrm{el}}/\partial \varepsilon_i'$. The expression for the elastic energy density of a cubic (110) film reads $f_{\mathrm{el}}=c_{12}[2\varepsilon_2'(\varepsilon_1'/2+\varepsilon_3'/2)+(\varepsilon_1'/2+\varepsilon_3'/2)^2] + c_{11}[\varepsilon_2'^2+2(\varepsilon_1'/2+\varepsilon_3'/2)^2]/2+2c_{44}(-\varepsilon_1'/2+\varepsilon_3'/2)^2$, with the elastic constants $c_{11}=229$ GPa, $c_{12}=134$ GPa, $c_{44}=115$ GPa.[18] Our experimental strain values lead to an in-plane stress of $\tau_1'=5.3$ GPa and $\tau_2'=4.7$ GPa, and to an out-of-plane stress $\tau_3'=3.1$ GPa. This has to be compared to the usual continuum elasticity approach with is characterized by $\varepsilon_3'(\mathrm{expected})=-0.0082$, and gives 4.6, 3.3, and 0 GPa, respectively. It is remarkable that the in-plane stress anisotropy is considerably smaller for the experimentally determined value of ε_3', as compared to its value for the calculated strain, $\tau_1'/\tau_2'=1.14$ vs 1.42. In earlier stress measurements of Fe films deposited on W(110), which were performed by the crystal curvature technique, we found an almost isotropic film stress of 13 GPa for films thicker than four monolayers.[18] This film stress was constant up to 10 ML thickness, which was the thickest film of that earlier study. From this earlier study we conclude that an isotropic film stress of this magnitude should also be expected for the 13-ML monolayer-thick film under investigation here. A comparison of the calculated stress, based on our strain values, with the measured stress of earlier curvature experiments indicates that the measured film stress (crystal curvature technique) exceeds the calculated value (based on film strain as derived from this x-ray diffraction study) by a factor of roughly 2.6. The larger magnitude of the experimental stress comes as a surprise, as in other systems such as Co or Ni on Cu(100) and Ag on Fe(100), the calculation of stress in several-monolayer-thick films with continuum elasticity leads to a good agreement with the experimental stress.[41] However, the much smaller stress anisotropy as calculated from the experimental strain is qualitatively in agreement with the isotropic stress, which we measured. We conclude that the Fe film stress cannot be adequately described by bulk continuum elasticity. We suggest that the magnitude of the bulk elastic constants be modified by the strain state of the film.

The film strain has a direct impact on the magnetic anisotropy via the magnetoelastic coupling. The large magnitude of the magnetoelastic coupling coefficients B_i of the order of several MJ/m^3 [$(B_1^{\mathrm{bulk}}=-3.43$ MJ/m^3 (-0.255 meV/atom), $B_2^{\mathrm{bulk}}=7.83$ MJ/m^3 (0.579 meV/atom)], which is roughly a factor of 100 larger as compared to the crystalline anisotropy,[6] makes magnetoelasticity an important contribution to the magnetic anisotropy in strained systems.[18] We discuss in the following section how the magnetic anisotropy of Fe monolayers is influenced by the strain state of the Fe film.

Fe monolayers on W(110) are a prototype of well studied systems,[6] where the magnetic anisotropy of monolayer thin films deviates from the bulk behavior. Bulk Fe has an easy magnetization direction along the cubic [100] directions, whereas in thin Fe films on W(110) an easy magnetization direction along in-plane $[\bar{1}10]$ is found, which was previously ascribed to the dominant contribution of a so-called surface anisotropy.[6] The easy magnetization direction reverts to the bulk easy magnetization direction [100] for Fe films thicker than approximately 50 ML.[6]

The following expressions give the contributions of the magnetoelastic coupling to the in-plane and out-of-plane anisotropy for cubic (110) films. The magnitude of the magnetic anisotropy energy density $f_{\text{mag-el}}$ is given as $f_{\text{mag-el}}^{\text{in plane}}=\frac{1}{2}(B_2-B_1)(\varepsilon_0'-\varepsilon_3')$ (in-plane $[\bar{1}10]$ vs in-plane [001], and a negative value indicates an easy magnetization direction along in-plane $[\bar{1}10]$).[6,19] We introduced the magnetoelastic coupling coefficients B_i, and we consider an isotropic in-plane strain $\varepsilon_0'=\varepsilon_1'=\varepsilon_2'$. Note that the difference between in-plane and out-of-plane strain $(\varepsilon_0'-\varepsilon_3')$ enters as a factor in the anisotropy expression. This reflects the physically sound idea, that the deviation from the cubic symmetry due to strain is essential for the magnetic anisotropy. In our case, both strain components $\varepsilon_0'=0.012$ and $\varepsilon_3'=0.0022$ are of the same sign, and their difference $\varepsilon_0'-\varepsilon_3'=0.01$ is smaller by a factor of 2 as compared to the difference calculated with the normal strain derived from continuum elasticity $\varepsilon_{3,\text{continuum elasticity}}=-0.0082$, $\varepsilon_0'-\varepsilon_{3,\text{continuum elasticity}}=0.02$. This demonstrates that a detailed knowledge of the strain state is essential for a proper anisotropy discussion.

The other factor (B_2-B_1) deserves also some special attention. The magnitude and sign of the magnetoelastic coupling coefficients B_i depend on the film strain,[18] and the appropriate value for Fe with $\varepsilon_0'=0.012$ is $B_1=1.5$ MJ/m^3.[18] Film stress-dependent measurements of B_2 have been performed by Wedler *et al.*, and extrapolating their values to our measured film stress of 13 GPa suggests $B_2=-14$ MJ/m^3.[40] Thus, $B_2-B_1=-15.5$ MJ/m^3, which differs in sign and magnitude from the respective difference calculated from the bulk values (+11.26 MJ/m^3). The consideration of the strain-dependent correction of the magnetoelastic coupling constants in connection with our strain analysis gives $f_{\text{mag-el}}^{\text{in plane}}=\frac{1}{2}(B_2-B_1)(\varepsilon_0'-\varepsilon_3')=-0.076$ MJ/m^3, which indicates an easy magnetization direction along in-plane $[\bar{1}10]$, which agrees with the direction of the easy magnetization axis of 13-ML Fe on W(110).[6] Elmers and Gradmann determined quantitative anisotropy values from torsion oscillation magnetometry,[6] and we derive from their data an in-plane anisotropy of -0.11 MJ/m^3 for 13 ML of Fe. This value agrees reasonably well with the anisotropy value as derived

from the magneto-elastic contribution (-0.076 MJ/m^3), and we conclude that the in-plane anisotropy of Fe films on W(110) can be ascribed to the magnetoelastic contribution to the anisotropy. The film strain is decisive for the magnetic anisotropy of the Fe monolayers. This conclusion does not require the introduction of significant surface anisotropy contributions, which were suggested as the driving force of the magnetic in-plane anisotropy of Fe layers on W(110).[6]

VII. SUMMARY

In summary we have presented a detailed SXRD analysis of a nominally 13-ML-thick Fe film deposited on W(110). The Fe atoms form a two-dimensionally modulated structure, which gives rise to a multiplet of satellite reflections. The analysis of both the satellite positions and their intensity allowed a thorough depth-resolved study of the modulated film. Our analysis indicates that the modulated Fe adlayer is ''incommensurate'' with the underlying W lattice (approximate 37/34 coincidence between Fe and W) and that the average Fe structure can be interpreted as a slightly laterally distorted bct phase. The modulation amplitudes within the film decrease with distance from the interface. For the lateral distortions we find maximum values in the 0.7-Å range for the vertical distortions values in the 1-Å range. These results are in fair agreement with previous LEED and STM work. A model for the registry between the Fe film and the W(110) surface proves the direct relation between the vertical corrugation and the local Fe adsorption site. We demonstrate that our strain analysis (in-plane film strain $\varepsilon_1'=\varepsilon_2'=0.012$; out-of-plane film strain $\varepsilon_3'=0.0022$), in conjunction with the strain-modified magnetoelastic coupling constants, offers a satisfactory description of the in-plane magnetic anisotropy of the 13-ML Fe film. We suggest the strain-induced anisotropy is the decisive factor for the magnetic anisotropy of this system.

ACKNOWLEDGMENTS

We (R.P., H.L.M., and D.S.) are grateful for the hospitality during our stay at the ESRF. The help of M. Dusek during the work with the Jana2000 program is gratefully acknowledged.

*Corresponding author. FAX: +49-345-5511-223. Email address: hmeyerhm@mpi-halle.de

†Present address: Department of Physics and Astronomy, E. C. Stoner Laboratory, University of Leeds, Leeds LS2 9JT, U.K.

[1] U. Gradmann and G. Waller, Surf. Sci. **116**, 539 (1982).

[2] G. Waller and U. Gradmann, Phys. Rev. B **26**, 6330 (1982).

[3] S. C. Hong, A. J. Freeman, and C. L. Fu, Phys. Rev. B **38**, 12 156 (1988).

[4] M. Przybylski, I. Kaufmann, and U. Gradmann, Phys. Rev. B **40**, 8631 (1989).

[5] M. Albrecht, U. Gradmann, T. Reinert, and L. Fritsche, Solid State Commun. **78**, 671 (1991).

[6] H. J. Elmers and U. Gradmann, Appl. Phys. A: Solids Surf. **51**, 255 (1990).

[7] H. J. Elmers, J. Hauschild, H. Höche, U. Gradmann, H. Bethge, D. Heuer, and U. Köhler, Phys. Rev. Lett. **73**, 898 (1994).

[8] H. J. Elmers, J. Hauschild, H. Fritsche, G. Liu, and U. Gradmann, Phys. Rev. Lett. **75**, 2031 (1995).

[9] H. Bethge, D. Heuer, Ch. Jensen, K. Reshöft, and U. Köhler, Surf. Sci. **331–333**, 878 (1995).

[10] Ch. Jensen, K. Reshöft, and U. Köhler, Appl. Phys. A: Mater. Sci. Process. **62**, 217 (1996); Ch. Jensen, Ph.D. thesis, Ruhr-Universität Bochum, Fakultät für Physik und Astronomie (1997).

[11] D. Sander, R. Skomski, C. Schmidthals, A. Enders, and J. Kirschner, Phys. Rev. Lett. **77**, 2566 (1996).

[12] N. Weber, K. Wagner, H. J. Elmers, J. Hauschild, and U. Gradmann, Phys. Rev. B **55**, 14 121 (1997).

[13] T. Dürkop, H. J. Elmers, and U. Gradmann, J. Magn. Magn. Mater. **172**, L1 (1997).

[14] E. D. Tober, R. X. Ynzunza, F. J. Palomares, Z. Wang, Z. Hussain, M. A. Van Hove, and C. S. Fadley, Phys. Rev. Lett. **79**, 2085 (1997).

[15] J. Hauschild, U. Gradmann, and H. J. Elmers, Appl. Phys. Lett. **72**, 3211 (1998).

[16] D. Sander, A. Enders, C. Schmidthals, D. Reuter, and J. Kirschner, Surf. Sci. **402–404**, 351 (1998).

[17] D. Sander, R. Skomski, A. Enders, C. Schmidthals, D. Reuter, and J. Kirschner, J. Phys. D **31**, 663 (1998).

[18] D. Sander, Rep. Prog. Phys. **62**, 809 (1999).

[19] D. Sander, A. Enders, and J. Kirschner, J. Magn. Magn. Mater. **200**, 439 (1999).

[20] D. Sander, A. Enders, and J. Kirschner, Europhys. Lett. **45**, 208 (1999).

[21] X. Qian and W. Hübner, Phys. Rev. B **60**, 16 192 (1999).

[22] F. C. Frank and J. H. van der Merwe, Proc. R. Soc. London, Ser. A **198**, 216 (1949).

[23] J. H. van der Merve, J. Appl. Phys. **34**, 123 (1963).

[24] J. H. van der Merwe and C. A. B. Ball, in *Epitaxial Growth B*, edited by J. W. Matthews (Academic, New York, 1975), Chap. 6.

[25] S. Brennan and P. Eisenberger, Nucl. Instrum. Methods Phys. Res. A **222**, 164 (1984); S. Ferrer and F. Comin, Rev. Sci. Instrum. **66**, 1674 (1994).

[26] H. L. Meyerheim, D. Sander, R. Popescu, P. Steadman, S. Ferrer, and K. Kirschner, Phys. Rev. B **64**, 045414 (2001).

[27] I. K. Robinson, Phys. Rev. B **33**, 3830 (1986).

[28] E. Vlieg, J. Appl. Crystallogr. **30**, 532 (1997); N. Jedrecy, *ibid.* **33**, 1365 (2000).

[29] R. Feidenhans I, Surf. Sci. Rep. **10**, 105 (1989).

[30] I. K. Robinson, and D. J. Tweet, Rep. Prog. Phys. **55**, 599 (1992).

[31] R. F. S. Hearmon, *The Elastic Constants of Crystals and Other Anisotropic Materials*, Vol. 18 of Landolt-Börnstein Numerical Data and Functional Relationships (Springer, Berlin, 1984).

[32] H. Schumann, *Kristallgeometrie* (Deutscher Verlag für Grundstoffindustrie, Leipzig, 1980).

[33] M. M. Woolfson, *An Introduction to X-Ray Crystallography* (Cambridge University Press, Cambridge, 1978).

[34] V. Petricek and M. Dusek, *Jana2000. The Crystallographic Computing System* (Institute of Physics, Praha, Czech Repulbic, 2000).

[35] A. Yamamoto, Acta Crystallogr., Sect. A: Found. Crystallogr. **A52**, 509 (1996).

[36] The unweighted residuum is defined as $R_u = \Sigma_{hkl} \| F_{hkl}^{\text{obs}} | - | F_{hkl}^{\text{calc}} \| / \Sigma_{hkl} | F_{hkl}^{\text{obs}} |$, where $|F_{hkl}^{\text{obs}}|$ and $|F_{hkl}^{\text{calc}}|$ are observed and calculated structure factor amplitudes, respectively. The summation runs over all measured reflections.

[37] U. Köhler (private communication).

[38] B. K. Vainshtain, V. M. Fridkin, and V. L. Indenbom, *Modern Crystallography II*, Vol. 21 of Springer Series in Solid State Sciences (Springer, Berlin, 1982).

[39] In this context it should be kept in mind that the situation is likely to be more complicated since the radii of the atoms depend on the coordination number and the different bonding character between Fe and W in the two sites.

[40] G. Wedler, J. Walz, A. Greuer, and R. Koch, Phys. Rev. B **60**, R11 313 (1999).

[41] D. Sander, S. Ouazi, V. S. Stepanyuk, D. I. Bazhanov, and J. Kirschner, Surf. Sci. **512**, 281 (2002); R. Mahesh, D. Sander, S. M. Zharkov, and J. Kirschner, Phys. Rev. B **68**, 045416 (2003); Th. Gutjahr-Löser, Ph.D. thesis, Universität Halle-Wittenberg (1999).